Atomistic simulation study of the diffusion and growth mechanisms of Ti thin films on Si(100) surfaces for betavoltaic cell

Hanzi Zhang,[1] Kaihong Long,[1] Yunze Han,[1] Chuankai Shen,[1] Menghe Tu,[1] and Baoliang Zhang[1, *]

[1]*China Institute of Atomic Energy, Beijing 102413, China*

The nucleation and growth behavior of Ti thin films on Si(100) surfaces at 500 K were investigated via molecular dynamics and Monte Carlo methods. The focus of this study was on the nucleation characteristics, growth mode, crystal structure and surface structure of the Ti thin films for use in betavoltaic cell. The results demonstrate that at the initial stage of deposition, mixing of Ti films with Si substrates occurs at the interface. The surface roughness of Ti films is influenced by the deposition atomic rate, which is associated with the crystal structure transition in the films, and the stable HCP grains in the films are frequently accompanied by an FCC laminated dislocation structure. As the deposition rate increased, the growth mechanism of the Ti films transitioned from a random orientation to a selective orientation. Furthermore, we recalculated the adsorption energies of Ti at different adsorption sites on the Si(100)p(2×2) surface. This was done to identify the optimal diffusion path of Ti atoms on the Si(100) surface, which was then found via the transition state search method.

Keywords: deposition; Si(100); Ti; first-principles calculation; molecular dynamics

I. INTRODUCTION

The interface between silicon and transition metals has long been highly important in various engineering applications, including microelectronic systems [1] and nanotechnology [2]. The electrical, thermal, and mechanical response of the silicon/transition metal interface is of paramount importance for the overall performance of the engineered system [3, 4]. In recent years, the field of nuclear energy has experienced a surge in interest in betavoltaic cell [5–7]. Betavoltaic cells offer a number of advantages, including a long operational lifetime, a stable output, ease of integration, a high energy density, and high environmental adaptability. As a result, betavoltaic cells are an ideal alternative in various situations where the use of fossil fuel or chemical batteries is not feasible, such as in remote sensing applications in extreme environmental conditions, medical implantable devices, and microelectromechanical systems (MEMS) [8]. Tritium betavoltaics hold more promise owing to the highly specific activity of solid tritium compounds, low shielding requirements and relatively high availability as a byproduct of CANDU® nuclear reactors [9]. A number of studies have been conducted on the incorporation of tritides into monocrystalline silicon transducers [10–12]. Tritiated titanium is renowned for its low decay ray energy, excellent chemical stability, and high safety. Titanium is capable of adsorbing and storing tritium in the solid-state at a pressure of approximately $1.33×10^{-5}$ Pa, forming tritiated titanium. This phenomenon results in a high storage density and rapid absorption rate of tritium. Equilibrium ionization decompression occurs at approximately 10^{-5} Pa at room temperature [13]. Samples containing silicon/transition metal interfaces are prepared via various vapor phase film growth techniques. The deposition of transition metals on monocrystalline silicon substrates is known to result in the formation of polycrystalline films. In fact, for the tritium betavoltaic cell with three-dimensional micro- and nanostructured semiconductors, existing studies have loaded tritium directly onto the semiconductors in the form of a gas, which requires exploring the possibility of obtaining tritium-absorbing metal thin films with the largest possible surface area and uniformly distributed in the three-dimensional micro- and nanostructures to act as tritium carriers, in order to obtain a higher amount of the radioisotope tritium. Ti thin films, as the tritium absorbing material in the betavoltaic cell, have a direct influence on the amount of tritium adsorbed and its diffusion path, thus affecting the energy conversion efficiency and output power density of the cell. The performance of tritium cells can be significantly improved by optimizing the Ti film preparation process.

Magnetron sputtering is a widely utilized technique for the deposition of titanium films. The preparation process is of great consequence with regard to the surface morphology, grain size, and texture of Ti films, thereby significantly impacting their functional properties [14–16]. Sputtering power is an important factor that influences the microstructure of titanium films by controlling the rate of atomic deposition. Chen et al. [17] demonstrated that the deposition rate has a significant effect on the microstructure of Ti films prepared by Si(100) surface magnetron sputtering. As the deposition rate increases, there is a transition from a random orientation to the (002) preferred orientation. Researchers have observed the nanoamorphous structure of the titanium film, characterized by the presence of nanocrystals within the amorphous matrix. Chawla et al. [18] reported that the grain size of a titanium film increased with increasing power and substrate temperature. At 100 W and 150 W, the preferred orientations of (101) and (002) on the glass substrate were observed. In a related study Han et al [19]. investigated the impact of sputtering powers ranging from 80 to 120 W on titanium thin films deposited in deep holes. These findings indicated that as the sputtering power increased, the thin films exhibited a tendency to form columnar structures. P. Moskovkin et al. [20] reported that at the lowest power density, the c axis of α-Ti[001] is perpendicular to the substrate, and the (002) plane is parallel to the substrate. As the discharge power density increases during deposition, additional Ti planes (100) parallel

* Corresponding author, zhangbaoliang@yeah.net

to the substrate appear. Finally, at the highest power density, a (100) plane parallel to the substrate is mainly observed during deposition. These structural changes cause changes in the hardness of the film. However, the cause of the (100) plane peak remains unclear. These studies have proposed a hypothesis regarding the nucleation and growth mechanism of Ti films on Si (100) substrates, but further research is still needed to study this process of deposition.

Atomic-scale simulations, including density functional theory (DFT), molecular dynamics (MD), and Monte Carlo (MC) simulations, have proven to be valuable tools for investigating the atomic-scale behavior of metal/ceramic interfaces, as well as for obtaining interfacial energetics [21–23], heat transport properties at interfaces [24], and dynamic processes at surfaces and interfaces [25, 26]. The first-principles method is highly accurate for the determination of energy changes and electronic information in the context of small system models. The team led by Rafael Añez employs first principles calculations to investigate the Ti atom adsorption process on the surfaces of Si (111) and Si (100) [21–23]. The interatomic interactions at the TiSi interface are analyzed from a thermodynamic perspective. The results indicate that the mixing of the TiSi interface is enhanced by defect regions on the substrate surface, thereby emphasizing the importance of Si diffusion in determining the structure of the TiSi mixed layer.

Over the past decade, MD simulations for plasma surface interactions have emerged as crucial tools for investigating a range of plasma phenomena, including sputtering, etching, injection, and deposition [27–30]. These simulations are capable of replicating the nucleation and growth behaviors of thin films. While periodic boundaries are commonly employed in MD simulations, ensuring that the model is sufficiently large to maintain the authenticity of the simulation is highly important. Moreover, variations in the type of element and the structure of the target within the simulation system can result in differences in the interatomic potential functions [31]. Conventional MD simulations are typically limited to scales of hundreds of nanoseconds due to the constraints imposed by the size of the simulated system and the interatomic potential function. Consequently, this limits the range of possible outcomes that can be observed in the simulation system, making it challenging to capture slow but critical structural evolution processes. Monte Carlo (MC) simulations determine atomic displacement probabilities on the basis of thermodynamic barriers, enabling a wider range of phase space sampling and often facilitating faster attainment of thermal equilibrium for surface structures [32–34]. Among the aforementioned algorithms, the primary advantage of the timestamped force–bias Monte Carlo (tfMC) method is its capacity to preserve the temporal scale. Although the tfMC method does not explicitly incorporate time, it establishes a correlation between simulations and time scales by integrating deterministic forces acting on atoms into a stochastic algorithm for atomic displacement. This results in a markedly increased acceptance rate of atomic displacement, thus accelerating the attainment of equilibrium in the simulated system. Reza Namakian and colleagues employed a sequential MD/time-stamped force–bias Monte Carlo (tfMC) algorithm to simulate the deposition behavior of copper (Cu) on a titanium nitride (TiN) substrate [26]. The transformation of the Cu film on the TiN (001) substrate from body-centered cubic (BCC) to face-centered cubic (FCC), accompanied by the formation of nanotwins, was observed and verified with experimental results. Furthermore, they identified distinct film growth mechanisms on the TiN(111) surface at the Ti-terminated end and the N-terminated end. Gao et al. [25] reported significant variations in the microstructures of Cu films deposited on different substrate surfaces. These variations were more pronounced on the Si(100) plane and in the vertical arrangement of higher-position atoms on the (110) crystal plane. Notably, specific deposition characteristics are observed on the (111) crystal face. Compared with the C (111) surface, the top atoms exhibit a more pronounced annular distribution and a relatively smooth surface. Considerable research has been conducted on the subject of MD simulations of Cu deposition on a Si substrate [35, 36]. However, studies on MD simulations for titanium films are scarce.

This study aims to investigate the nucleation and growth mechanisms of a Ti film on a Si (100) substrate via computational simulation. The primary objective of this study is to analyze the impact of different deposition energies on the microstructure of Ti films and the process of Ti nucleation and growth on Si (100) substrates. Section 2 provides a comprehensive account of the computational methodology employed in this study and the model configuration. The principal simulation outcomes are presented and discussed in Section 3, followed by a summary in Section 4.

II. COMPUTATIONAL DETAILS

A. DFT

All density functional theory (DFT) calculations were performed via DS-PAW software [37]. The Perdew–Burke–Ernzerhof (PBE) generalized gradient approximation (GGA) is employed to handle the exchange correlation between electrons. A plane wave cutoff of 400 eV is utilized in all calculations, with a vacuum layer set to 15 Å in the Z direction of the geometry. The Methfessel–Paxton integration scheme is employed for sampling the Brillouin zone at Monkhorst–Pack special points [38]. The following calculation was performed with an energy convergence criterion of 10^{-6} eV and a force convergence criterion of 0.01 eV·Å^{-1}. The atomic adsorption energy is determined through the following calculation:

$$E_{ads} = E_{Si(100)+nTi} - E_{Si(100)+(n-1)Ti} - E_{Ti}, \quad (1)$$

where $E_{Si(100)+nTi}$ denotes the energy of the surface containing n adsorbed Ti atoms, $E_{Si(100)+(n-1)Ti}$ denotes the energy of the surface of (n-1) adsorbed Ti atoms, and E_{Ti} is the energy of the ground state of an isolated Ti atom.

To gain further insights into the adsorption and diffusion behavior of Ti on the Si(100) surface, this study employs

the transition state search (TSS) method to calculate the optimal diffusion paths and the corresponding energy barriers between different adsorption sites. Additionally, the k-point mesh utilized for climbing-image nudged elastic band (CI-NEB) calculations is set at $6 \times 6 \times 1$, while the convergence criterion for energies is maintained at a constant value. Conversely, the criterion for forces is modified to 0.01 eV·Å^{-1}.

B. Model of titanium atom deposition and simulation methodology

All the MD simulations were conducted via the large-scale atomic/molecular massively parallel simulator (LAMMPS) [39]. A Si(100) surface structure was constructed as a substrate via LAMMPS, with the x, y, and z axes oriented in the [011], [0$\bar{1}$1], and [100] directions, respectively, and with a model size of $69 \times 69 \times 154$ Å^3 containing a total of 12,960 Si atoms. The x- and y-directions were subject to periodic boundary conditions, which enables the substrate to be treated as an infinite flat plate in the xy-plane. In contrast, the z-direction was subject to a fixed boundary condition. The existence of dimers on the (100) surface of Si introduces a certain degree of randomness to the surface arrangement [0$\bar{1}$1]. To obtain the final substrate surface structure for the atomic deposition simulation containing dimers, the initial surface relaxation of Si(100) was carried out under the NPT system for 100 ps. Fig. 1 depicts the simulated surface model of Ti deposition on a single-crystal Si(100) substrate. The substrate is represented by a fixed layer, a temperature-controlled layer, and a free layer from the bottom to the top. The fixed layer was established to prevent momentum transfer when the incident atoms collide with the substrate, thereby preventing the model from drifting. The top eight layers of atoms in the substrate are designated free layers, allowing for unrestricted interactions with incident particles to simulate the diffusion behavior of atoms at the Ti–Si interface during the deposition process. Upon impact with the substrate, the incident particles interact with one another, imparting kinetic energy to the system. This energy is subsequently converted into latent heat of condensation, resulting in an increase in the system temperature. To maintain a constant temperature throughout the deposition process, different system combinations were employed for different layers of the model. These combinations were designed to regulate the temperature within the system.

Relevant studies have demonstrated that the relaxation process in vapor deposition simulations significantly impacts the final microstructure of thin films. To more accurately simulate the growth behavior of Ti atoms on the surface of Si (100) during deposition, this paper employs a simulation scheme that combines the timestamped force-bias Monte Carlo (tfMC) method and MD. The tfMC approach does not consider atomic velocity; therefore, its practical significance lies in the sampling temperature of the system rather than the traditional temperature. The key parameter for determining the success of a tfMC simulation is the maximum displacement length Δ of the lightest element in the system. A larger
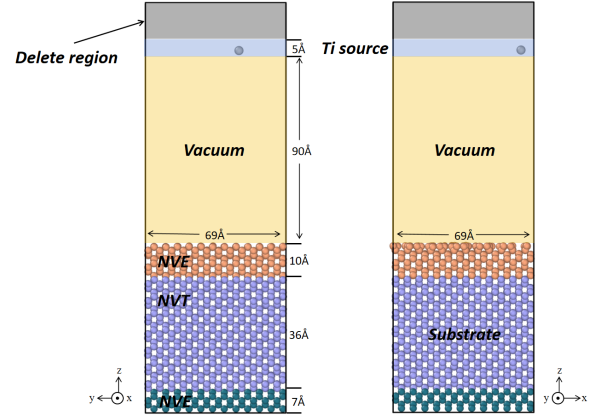

Fig. 1. Model employed for simulating the deposition of Ti on a Si (100) substrate

Δ results in a longer effective timescale for simulation. However, Δ must also be selected to be sufficiently small to meet equilibrium requirements. In this work, the properties of perfect lattice titanium and semiconductor silicon were tested separately. The results indicate that conditions with ΔTi = 0.1 and ΔSi = 0.1 ensure an increased sampling phase space while maintaining minimal precision loss.

C. Simulation of titanium atom deposition

The deposition process is divided into two stages: the first involves mutual diffusion between Ti and Si atoms, whereas the second involves self-diffusion of deposited Ti atoms. To accurately depict the deposition behavior and investigate the film growth mechanism, we utilize the Tersoff potential function developed by Plummer et al. [40] to describe the interaction between Ti and Si , in conjunction with the EAM potential function developed by Mendelev et al. [41] to characterize the interactions between Ti atoms. Prior to the commencement of the formal simulation, a validation of a hybrid scheme incorporating both potential functions was conducted. To facilitate the study, we assumed that the incident particle approaches the surface at a velocity perpendicular to it. Depending on the specific deposition parameters, a Ti atom is randomly emitted to the substrate within the incident layer. The velocity of the incident atom is determined by the given incident energy E_{in}, which can be calculated as follows:

$$v = \sqrt{\frac{2E_{in}}{m}}, \tag{2}$$

where v represents the velocity of the incident particle and m represents the mass of the incident particle. The incident energy range in this paper is 0.01 eV to 20 eV, with several values selected for simulation. Table. 1 shows the incident energy of the Ti atom.

The substrate temperature was set to 500 K during the thin-film deposition process. The temperature of 500 K was se-

TABLE 1. Velocity of the incident atoms.

energy(eV)	rate($\text{Å}\cdot ps^{-1}$)
0.1	6.3
0.5	14.2
1	20.1
5	44.9
10	89.8

lected based on its capacity to provide the optimal kinetic energy for promoting film growth during Ti deposition. The diffusion behavior of Ti atoms is more significant at this temperature, which affects the orientation, nucleation, and growth process of the film, ultimately resulting in a higher quality film.Furthermore, a series of control experiments were conducted at 300 K and 0.1 eV to investigate the phase transition phenomenon during the growth of Ti films. The system achieved thermal equilibrium by undergoing a 20 ps relaxation period under the NVE ensemble before the deposition process was initiated. For the Nose–Hoover thermostat and Nose–Hoover barostat, the time constants for temperature and pressure relaxation toward the desired values were set to 100 and 1000 times the timestep, respectively. A specified number of Ti atoms were randomly inserted in the deposition area, with each newly deposited atom required to be at least one cutoff radius (6.9 Å) away from the previously deposited atom. Following the completion of the deposition process, an NVT ensemble relaxation was employed to regulate temperature fluctuations resulting from kinetic energy transfer during successive collision events of the deposited Ti atoms. To ensure the comprehensive execution of both types of diffusion processes in the deposition simulation, 50 cycles were carried out, with 300 atoms per deposition cycle. Therefore, each cycle consisted of MD deposition, MD thermal balance, tfMC relaxation, and MD thermal balance. Visualization of all the simulation results was performed via OVITO software. The surface atomic structure was analyzed via the polyhedral template matching (PTM) method, with the RSMD cutoff set to 0.1.

III. RESULTS AND DISCUSSION

A. Ti diffusion behavior on the Si(100) surface

The cubic Si bulk was initially optimized, and the energy and force converged under a Monkhorst-Pack mesh of 4 × 4 × 4 K-points. The optimized lattice constant is 5.47 Å, which is in agreement with the results reported by Rafael Añez et al. [23] and experimental data (5.43 Å) [42], with an error of no more than 1%. The structure-optimized Si(100) surface, which contains four Si dimer structures, is depicted in Fig. 2. The Si atoms in the dimers are shown in distinct colors for ease of differentiation. The structure was obtained by cell expansion and modification of the cut surface on the basis of Si(100)p(2×2). The Si(100) surface model used in this work has a total of 8 layers of atoms. The formation energy of the

dimers on this surface is 1.68 eV, and these dimer structures are highly similar. Furthermore, the x, y, and z directions of the model correspond to the [010], [001], and [100] directions of the Si crystal, respectively. The dangling bonds on the bottom surface are saturated by hydrogen atoms. The bottom four layers of atoms are fixed in subsequent calculations to simplify the model. Such a research approach has been demonstrated to be feasible on numerous occasions. Additionally, the k-point mesh utilized for calculations is set at 6 × 6 × 1.
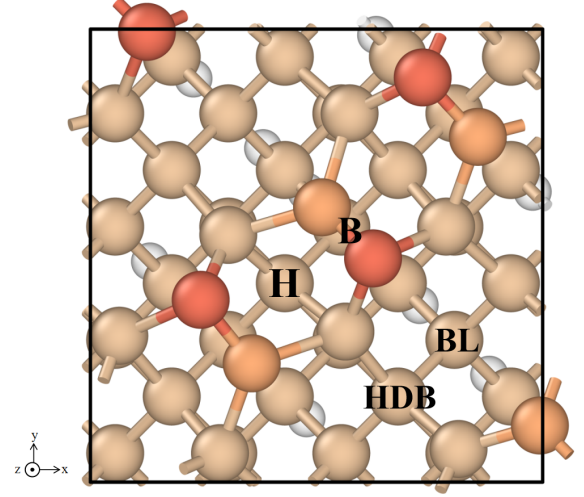

Fig. 2. Si(100) surface model, which comprises a tetrameric unit; the higher Si atom is designated by an orange–red color, whereas the other is designated by an orange–yellow color for ease of visual observation.

The dimer structure of the Si(100) surface results in the existence of four distinct adsorption sites for individual Ti atoms on the periodic substrate, which are labeled with letters in Fig. 2. The adsorption energies of individual Ti atoms on different sites on the Si(100) surface are presented in Table. 2. Among the four sites, site B is energetically less stable, and its structure optimization results are similar to those of site H, which will not be considered subsequently.

TABLE 2. Ti adsorption energies (eV) at different sites.

Atom/Position	Adsorption energy
H	-5.65
HDB	-4.36
BL	-4.96
B	

The results indicate that Ti atoms are most favorable for adsorption at the H-site, with an adsorption energy of -5.65 eV. The Ti atoms at the H-site are bonded with Si atoms in the four surrounding dimers. There are two types of Ti-Si bonds, with bond lengths of 2.40 Å and 2.42 Å, as shown in Fig. 3(a, b). The bond length between the Si atoms in the dimer is observed to increase as a consequence of the interaction between the Ti-Si atoms. Concurrently, the asymmetry of the Si

atoms in the two dimers bonded to them is reduced because of the adsorption of Ti atoms at the HDB sites. Nevertheless, the atomic environments of the two are not equivalent, and the bond lengths of the Ti–Si bonds are still different, measuring at 2.67 Å and 2.53 Å. This is not consistent with the results reported by Rafael Añez et al. This discrepancy can be attributed to the fact that the surface model in this paper has a larger periodic unit. The structures of Ti atoms adsorbed at the H and HDB sites exhibit a relatively low degree of symmetry, which is influenced by the presence of neighboring dimers. Consequently, the calculations presented in this paper are more consistent with the adsorption properties of individual Ti atoms on the Si(100) surface. When the Ti atom adsorbs on the BL site, the Si atoms bonded to the Ti atom exhibit three distinct atomic environments. The Ti atom interacts with the Si atoms on the two subsurfaces of the nondimer (Fig. 3e, f) with a bond length of 2.60 Å. Furthermore, this Ti atom is bonded to the Si atoms of the two neighboring dimers. In fact, the two Si atoms have different atomic environments. In contrast to the surface model presented in Refs. [23], the adsorption sites are positioned as far as possible within the interior of the model rather than on the periodic boundaries. This approach ensures the acquisition of more realistic adsorption energy data.Changes in the bond length between Ti and Si affect the electron density distribution and local geometry between them, which in turn changes the electron supply capacity of the adsorption sites. In the case of short Ti-Si bond lengths, the increased electron density in the vicinity of Ti atoms further facilitates the electron transfer from the adsorption sites, thus decreasing the adsorption energy. Conversely, as the Ti-Si bond length increases, the electron density decreases and the adsorption energy is relatively elevated.

Fig. 3. Adsorption positions of Ti at the H (a, b), HDB (c, d) and BL (e, f) sites (top view and view along the positive xy direction).

The precise calculation of the adsorption energy of individual Ti atoms enabled the determination of the minimum energy paths for the diffusion of Ti atoms from the first nearest neighboring HDB and BL sites to the H site. Five points were set between the initial and final positions via linear interpolation. The results of the transition state search are presented in Fig. 4. The diffusion of Ti atoms from the HDB site to the H site necessitates the crossing of the Si atoms in the two dimers to which they are bonded. As previously discussed, the two Si atoms regain some symmetry under the influence of the Ti atom at the HDB site. Consequently, at this juncture, the Ti atoms diffuse in a roughly linear trajectory toward the H site. The system energy reaches its maximum when the Ti atom is directly above the two Si atoms. Notably, the calculated shortest diffusion path from the BL site to the H site reveals that the Ti atoms must traverse two potential barriers throughout the entire process. The Ti atoms initially reach the first nearest-neighbor HDB site and subsequently diffuse to the most stable H site. These results indicate that the adsorption of Ti atoms at the H site on the Si (100) surface is highly stable and that the diffusion of Ti atoms requires overcoming a high potential barrier.
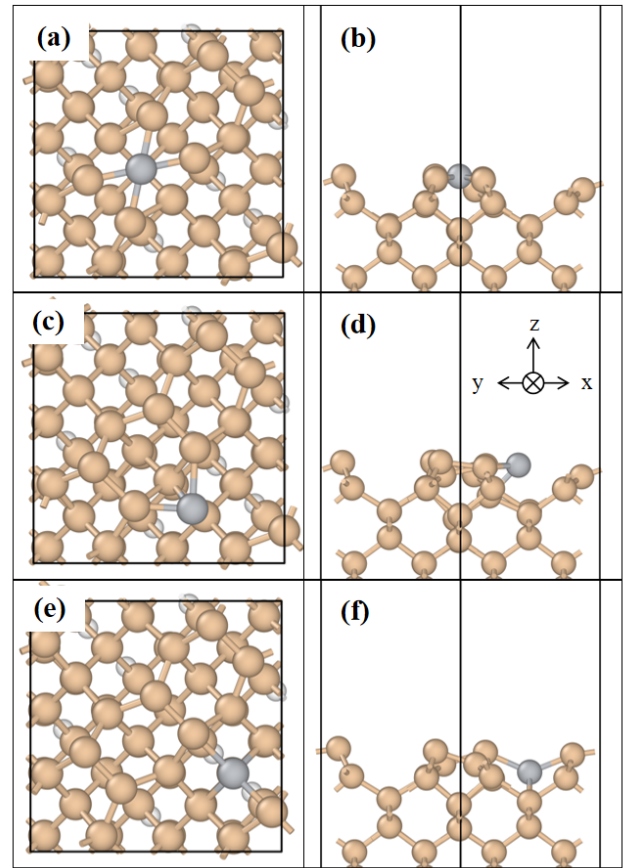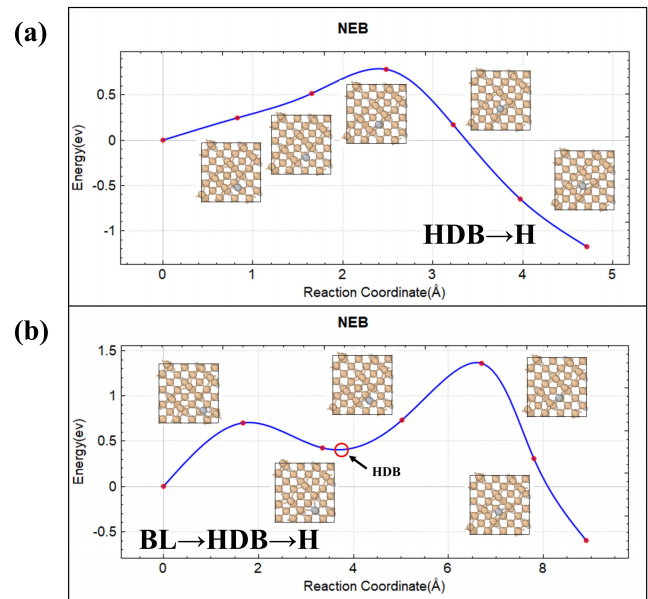

Fig. 4. Diffusion barriers and diffusion paths of Ti between different adsorption sites: (a) HDB→H and (b) BL→HDB→H.

B. Molecular dynamics/Monte Carlo simulations of Ti deposition
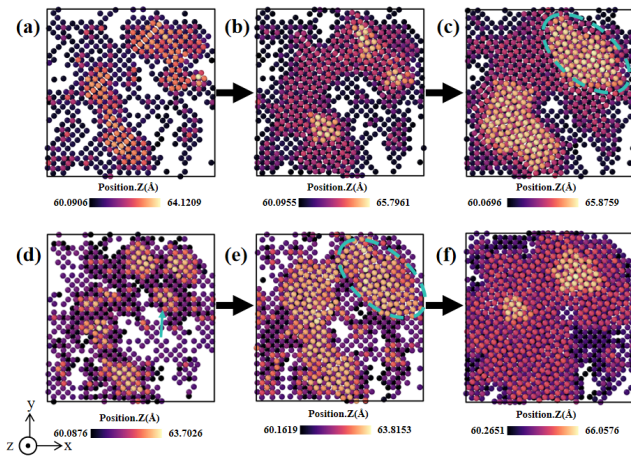

Fig. 5. Island growth patterns during the initial stages of film deposition at different incident energies. (a-c) 0.1 eV, 4–6 loop. (d-f) 5 eV, 4–6 loop.

In accordance with the deposition scheme outlined in Section 2, we proceeded to deposit 15,000 atoms on the Si(100) surface in approximately 25 layers. The interval of incident atomic energy was considered to be 0.1 eV to 5 eV. Fig. 5 shows the initial island growth and island aggregation behavior of the Ti films at incident energies of 0.1 eV and 5 eV. To quantify the changes in the deposition structure over time, we chose to use the number of simulated cycles as a proxy for the simulation time in our analysis. At the beginning of the deposition simulation, Ti atoms readily form 3D islands locally (Fig. 5(a, d)) because of the adsorption of Ti on the Si(100) surface. At low energy incidence, the islands gradually coalesce, resulting in two-dimensional growth in the xy plane with minimal change in island height. As the islands continue to grow in two dimensions, the film thickness increases. The islands merge and gradually wet the entire substrate, as illustrated in Fig. 5(b) and Fig. 5(c). In the case of high-energy incidence, the distribution of Ti atoms is slightly deeper, as illustrated in Fig. 5(e). In other words, the surface is covered with Ti atoms at an earlier stage in the case of high energy incidence, leading to the subsequent stage of film growth occurring at a faster rate. In the subsequent stage, the stacking of Ti atoms is the primary mode of growth, resulting in a notable increase in the rate of film growth [43]. In addition, the layer coverage of Ti and Si atoms near the Ti–Si interface (position. Z = 60) was quantified (Fig. 6). To eliminate the possibility of random results, the coverage results were compared between the 20% and 80% intervals. The results show that the diffusion of Si and Ti is not significant in the low-energy deposition state. When the incident energy is high, Ti atoms produce a better ion implantation effect. As a d element, the lower mixing ratio of Ti to Si is analogous to the Co to Si study [44]. Despite the lower mixing ratio at the interface, a minimal quantity of Si still exerts a modicum of influence on the growth of Ti films. The detachment of Si forms irregular defects at the interface that may act as sites for preferential nucleation of Ti atoms. Following the initial nucleation event, the deposition of Ti atoms continues around these defect sites, resulting in a film growth pattern that exhibits specific orientations or the formation of early grain boundaries and stress concentration regions.

Fig. 7 shows the evolution of the crystal structure in the Ti films as a function of simulation time at different incident energies. The results show that Ti films deposited on Si(100) surfaces at 500 K eventually form the HCP structure, which accounts for up to 60% of the crystal structure statistics. At high sputtering power, Ti migrates on the substrate surface and occupies an available equilibrium position on the pre-existing titanium film lattice, resulting in the formation of a columnar structure in the film [45]. The film grows at an inclined angle, which is consistent with the results of other studies [46]. During the initial stages of film deposition, the Ti films predominantly exhibit the BCC phase. After 10 cycles, the substrate surface becomes covered with Ti atoms, indicating that the growth of the Ti thin films had entered the Ti stacking phase. At this stage, the formed Ti film is influenced by the surface structure of the Si(100) substrate. The atomic arrangement is looser, and the space utilization is lower. At this stage, the Ti films form local BCC structures on the surface. These structures act as buffer regions between subsequent HCP structures and the Si substrate until the HCP structures at higher locations reach a certain level before disappearing. Notably, the stable growth phase of HCP structures is often accompanied by the formation of FCC layer defects, which greatly enhance the stability of the HCP structures. At an incident atomic energy of 20 eV, a higher deposition energy leads to more pronounced local emergence of the BCC structure. Owing to the more active local atomic environment, the formation of FCC layer defects was not observed in the initial HCP structures. These structures remain unstable and undergo significant compositional fluctuations during further deposition and relaxation processes.

The surface topographies of the Ti films at different incident energies were analyzed, showing that the four surfaces at lower energies (Fig. 8(a-d)) exhibited similar surface topographies and banded grains, which were oriented in both the (002) and (101) directions. This is due to the earlier formation of layer mismatches in the films under low-energy deposition, which leads to incomplete relaxation of the crystal structure. The Ti film at an incident energy of 20 eV in Fig. 8(e) has larger grains. Moreover, the films deposited with an incident energy of 20 eV exhibited a uniform (101) surface orientation. This suggests that the (101) surface has a higher priority than the (002) surface at high temperatures (500 K). This finding is consistent with the findings of Chawla et al. [18].

To further illustrate the effect of incident energy on the surface quality of thin films, this paper employs the metric of surface roughness to quantify this difference. Surface roughness is a common descriptor of the microscopic morphology of a film, and it affects the film's properties to some extent. Typically, the lower the surface roughness is, the greater the resistance and oxidation resistance. As the incident energy
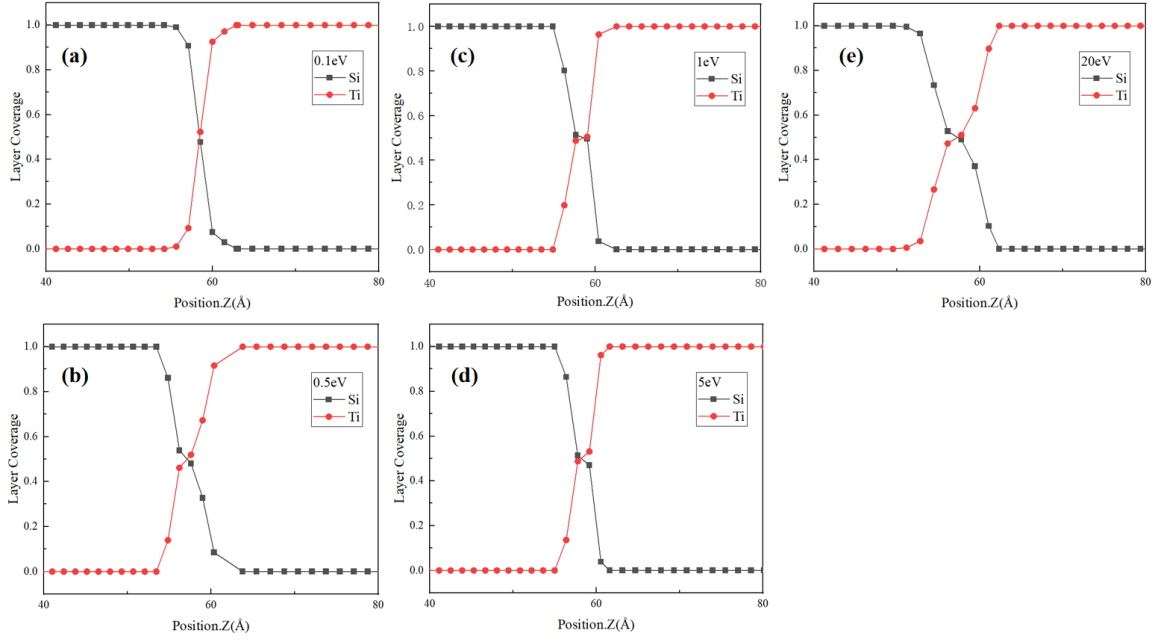
Fig. 6. Layer coverage of Ti and Si in the final Ti films at different incident energies. (a) 0.1eV, (b) 0.5eV, (c) 1eV, (d) 5eV, (e) 20eV.
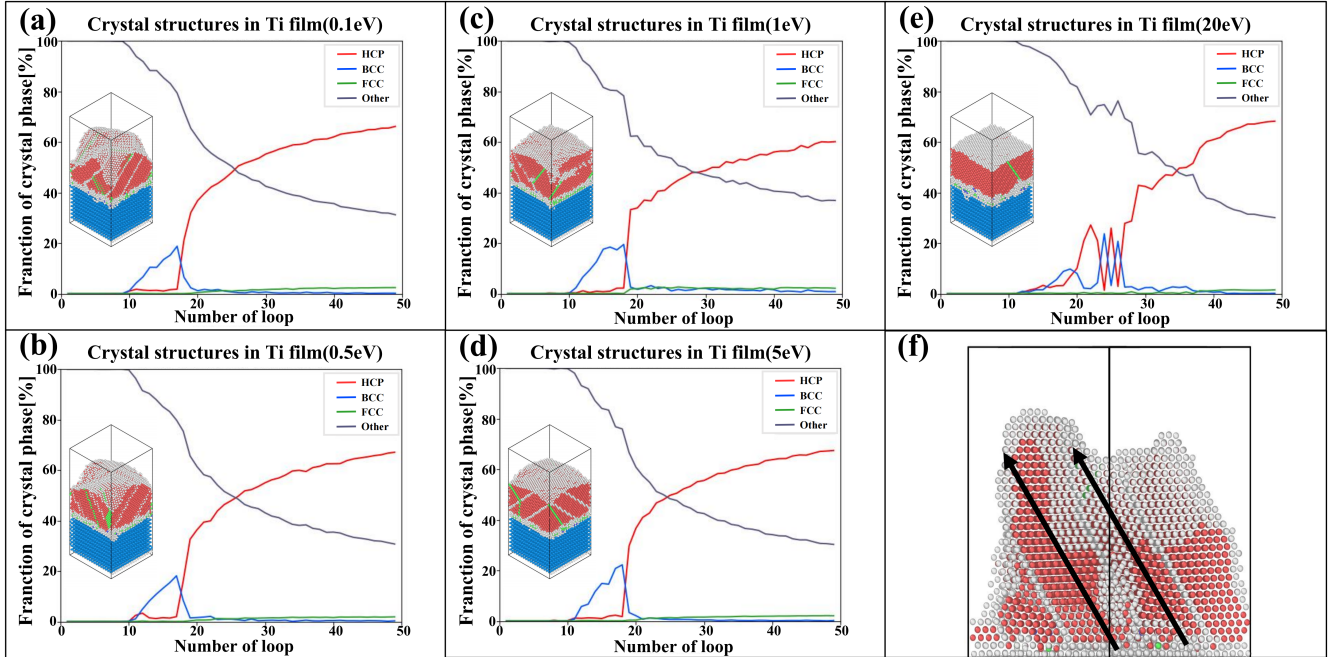

Fig. 7. Variation in the crystal structure of the Ti films with increasing number of cycles at different incident energies. (a) 0.1eV, (b) 0.5eV, (c) 1eV, (d) 5eV, (e) 20eV. (f) Tendency of thin growth. The different crystal structures are distinguished in the figure via the PTM method, with red denoting the HCP structure, green denoting the FCC layer dislocations, and gray denoting the amorphous structure.

increases, the surface roughness also increases, which in turn alters the diffusion paths and nucleation mechanisms of Ti atoms to some extent. The presence of diverse nucleation sites on high-roughness surfaces results in a more randomized and denser nucleation of Ti. Additionally, the concave and convex structures on rough surfaces prolong the retention time of the atoms, potentially contributing to the emergence of three-dimensional island growth modes and influencing the overall quality and homogeneity of the films. In the molecular dynamics simulations presented in this paper, the surface roughness of the film was calculated from the z-coordinate of the atoms on the surface of the film, which is expressed by
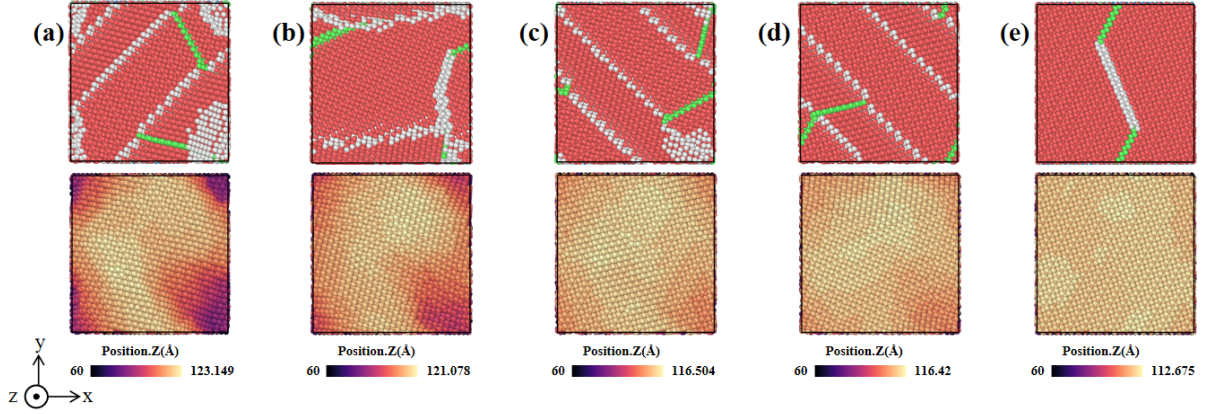
Fig. 8. Cross-sections (Position. Z = 100) and the surface morphology of the films with different incident energies. (a) 0.1eV, (b) 0.5eV, (c) 1eV, (d) 5eV, (e) 20eV. The PTM method has been used to distinguish the different crystal structures in the cross-sectional view, with red denoting the HCP structure, green denoting the FCC layer faults, and gray denoting the interface.

the root-mean-square roughness R. The surface roughness of the film can be calculated from the z-coordinate of the atoms on the surface of the film [47]:

$$R = \sqrt{\frac{\sum_{i=1}^{N}(Z_i - \overline{Z})^2}{N}}, \tag{3}$$

where i is the surface atom of the deposition layer and its number is N. Z_i represents the height of the surface atom of the deposition layer, whereas $\overline{Z}$ denotes the average height of all the surface atoms. The resulting calculations are presented in Fig. 9.
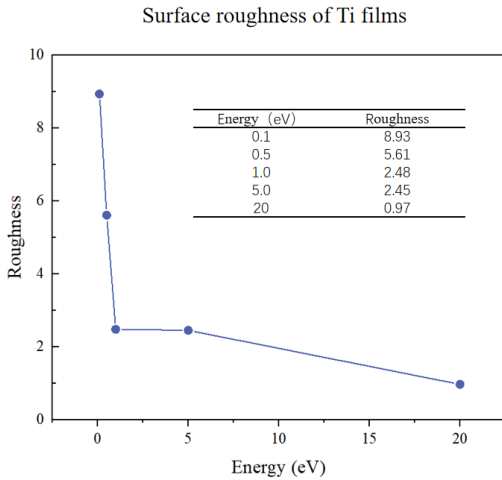

Fig. 9. Surface roughness of Ti films at different incident energies

The results demonstrate that the incident atomic energy profoundly influences the final surface roughness of Ti films. At lower energy states, increasing the energy of the incident atoms has a markedly beneficial effect on the surface roughness of the films. However, this effect diminishes as the incident energy increases from 0.1 eV to 5 eV, reaching a plateau period. When the incident energy was increased to 20 eV, the surface roughness decreased further to 0.97. We believe that the main factor for the first decrease in surface roughness is the surface diffusion of Ti atoms during deposition, and the second decrease is the result of grain merger at high energy. The incident energy of the deposited atoms exerts a pronounced influence on the surface roughness of the resulting film. An increase in surface roughness can facilitate the formation of additional sites for tritium adsorption. However, it should be noted that larger surface roughness also gives rise to the generation of more intricate nucleation sites during the process of film growth. This, in turn, has the potential to influence the film's intrinsic properties, including its thickness uniformity and grain size. It is therefore our contention that a distributed deposition method can be employed to regulate the quality of the film by utilizing disparate incident energies throughout the deposition process.

C. Ti diffusion behavior on the Si(100) surface

Selective surface orientation behavior generally occurs during the deposition of Ti thin films. Moskovkin et al. [48] revealed that during the deposition process, the Ti(002) plane parallel to the substrate is generated in the low-energy state, whereas the (100) plane parallel to the substrate is mainly observed in the high-energy state. To investigate the reasons for this phenomenon, we conducted deposition simulations at 300 K and 0.1 eV, and obtained surfaces containing (002) planes without (100) planes. The results are shown in Fig. 10(a). Unlike the 500 K simulation, there is no production of BCC nanocrystals in this simulation. This indicates that the surface orientation of Ti (100) is generated by the BCC nanocrystalline phase transformation, and this transformation process shown in Fig. 10 (c-e) is also consistent with the mechanism of Ti metal phase transformation [49, 50]. During the phase transition process, the lattice undergoes a large deformation along the $\beta[110]$ direction. Since the film
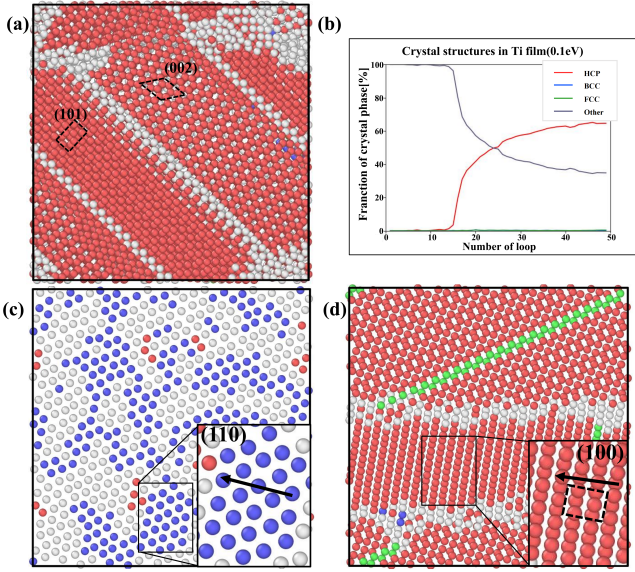
Fig. 10. (a-b) Film cross-sections and changes in the crystal structure at 300 K and 0.1 eV. (c-d) Film cross section at 500 K and 0.1 eV. The PTM method has been used to distinguish the different crystal structures in the cross-sectional view, with red denoting the HCP structure, green denoting the FCC layer faults, and gray denoting the interface.

has a larger relaxation space in the Z-axis direction, the $\beta \rightarrow \alpha$ phase transition tends to align the $\alpha(100)$ plane parallel to the substrate rather than the (002) plane, resulting in the preferential formation of the (100) plane. In addition, we also calculated the surface energies of BCC(110), HCP(002), and HCP(100). The surface energies of HCP-Ti and BCC-Ti are given by:

$$E_S = \frac{1}{2A}(E_{slab} - \frac{N_{slab}}{N_{bulk}}E_{bulk}), \qquad (4)$$

where A is the surface area, E_{slab} is the slab energy with N_{slab} atoms, and E_{bulk} is the bulk energy with N_{bulk} atoms. The value of 2A is related to two surfaces of a slab.

In the process of calculating the surface energy, we adopted a truncation energy consistent with that mentioned above and tested the convergence of different layers and different K-points. The final calculation results are shown in Table 3. These results indicate that $\alpha(100)$, as a close-packed surface of HCP-Ti, has a higher surface energy. We believe that the lattice deformation caused by the phase transition is the direct cause of the selective surface orientation and that the energy stability of the surface is the fundamental cause of the selective surface orientation. The ambient temperature during thin film deposition has an impact on the crystal structure and surface orientation of the resulting film. To enhance the energy conversion efficiency and output power density of tritium cells, it is essential to ensure that the metal films possess a robust crystal structure and optimal surface orientation, which enables effective tritium adsorption and osmotic diffusion. It must be acknowledged that the processes of tritium adsorption and permeation-diffusion are highly complex, and further studies are required to ascertain the full extent of these effects. Our findings demonstrate, however, that experimenters can exert partial control over the crystal structure and surface orientation of Ti metal films by regulating the ambient temperature.

TABLE 3. The surface energies (eV) at different sites.

Surface	Surface energy(J·m^{-2})
$\beta(110)$	1.75
$\alpha(002)$	1.96
$\alpha(100)$	2.03

IV. CONCLUSION

The objective of this work is to investigate the diffusion and deposition behavior of Ti on the Si(100) surface at the atomic scale through the use of atomic scale simulations. A more realistic surface model was employed to calculate the adsorption energies of Ti atoms at different adsorption sites on the Si(100) surface. This resulted in the identification of the optimal path for the diffusion of Ti atoms on the surface. The atomic deposition simulation results indicate that Ti atoms strongly prefer to occupy the entire surface, with this process being regulated by the two-dimensional diffusion of Ti atoms. The nucleation of Ti films is influenced by the upward-diffusing Si atoms, with the stable HCP grains in the films often accompanied by an FCC laminated dislocation structure. The surface roughness of the Ti films gradually decreases with increasing incident energy, which is related to the crystal structure transition in the films. Our study concludes that regulating the incident energy during deposition can effectively control the surface roughness of Ti films, thereby influencing the film's thickness uniformity and grain size. In addition, the direct reason for the formation of the (100) surface in the film is lattice deformation during the phase transition of the BCC nanocrystalline material, and the fundamental reason is that the (100) surface itself has a more stable structure. By regulating the ambient temperature during deposition, it is possible to influence the crystal structure and surface orientation of Ti thin films, which is crucial for enhancing the performance of tritium betavoltaic cells.

V. CREDIT AUTHORSHIP CONTRIBUTION STATEMENT

Hanzi Zhang: Methodology, Software, Validation, Formal analysis, Investigation, Data curation, Visualization, Writing – original draft. **Kaihong Long**: Software, Validation, Formal analysis, Visualization, Writing – review & editing. **Yunze Han**:conceptualization, visualization. **Chuankai Shen**: conceptualization, visualization. **Menghe Tu**: Conceptualization, Validation, Investigation, Data curation, Writing – review & editing. **Baoliang Zhang**:

Writing – review & editing, supervision, project administration, funding acquisition.

[1] H.K. Cheemalamarri, S. Bonam, S.R.K. Vanjari et al., Ti/Si interface enabling complementary metal oxide semiconductor compatible, high reliable bonding for inter-die micro-fluidic cooling for future advanced 3D integrated circuit integration. J. Micromech. Microeng. **30**, 105005 (2020). doi:10.1088/1361-6439/ab9f00

[2] N. Benito, C. Palacio, Growth of Ti-O-Si mixed oxides by reactive ion-beam mixing of Ti/Si interfaces. J. Phys. D: Appl. Phys. **47**, 015308 (2014). doi:10.1088/0022-3727/47/1/015308

[3] G. Saheli, T. Kuratomi, I.C. Chen et al., Use of Si KLL Auger shifts and the Auger parameter in XPS to distinguish Ti silicides from a Ti/Si mixture in thin films. J. Electron Spectrosc. Relat. Phenom. **234**, 57-63 (2019). doi:10.1016/j.elspec.2019.04.004

[4] Z.Y. Zhao, Y Liu, B Zhou et al., Wettability and joining of reaction-bonded silicon carbide (RBSC) by Ti–Si eutectic alloy. Ceram. Int. **50**, 21184-21192 (2024). doi:10.1016/j.ceramint.2024.03.227

[5] X.Y. Wang, J.M. Feng, H.J. He et al., Modified graphene by 1 MeV electron irradiation in betavoltaic cell. Nucl. Instrum. Methods Phys. Res., Sect. B. **554**, 165410 (2024). doi:10.1016/j.nimb.2024.165410

[6] B. Han, Z.S. Wang, D. Neena, et al., Influence of N_2 flow rate on structure and properties of TiBCN films prepared by multi-cathodic arc ion plating and studied with ion beam scattering spectroscopy. Nucl. Sci. Tech. **28**, 59 (2017). doi:10.1007/s41365-017-0212-0

[7] J.C. Zhang, Y.C. Han, L. Ren et al., Design and Preparation of SiC Radiation Voltaic Isotope Battery. At. Energy Sci. Technol. **55**, 182 (2021). doi:10.7538/yzk.2020.youxian.0896

[8] C.L. Zhou, J.S. Zhang, X. Wang et al., Review—Betavoltaic Cell: The Past, Present, and Future **10**, 027005 (2021). doi:10.1149/2162-8777/abe423

[9] B.L. Ellis, H. Fritzsche, J. Patel et al., Titanium tritide films as betavoltaic power sources. J. Electron. Spectrosc. Relat. Phenom. **71**, 660-665 (2017). doi:10.1080/15361055.2017.1290952

[10] Y.Q. Yang, Y.S. Lei, Z.K. Zhong et al., Long-Term Stability of Betavoltaic Battery Model and Prototype Based on Tritium/C-Silicon PN Junction Devices. J. Isot. **34**, 10-15 (2021). doi:10.7538/tws.2021.34.01.0010

[11] X. Li, G.Q. Wang, Y.Q. Yang et al., Initial Research in Composite Electrodes with Energy Storage Applied for Betavoltaic Isotope Battery. At. Energy Sci. Technol. **52**, 175-180 (2018). doi:10.7538/yzk.2018.52.01.0175

[12] X.Y. Wang, J.M. Feng, H.J. HE et al., Effect of Different Modification Methods on the Output Performance of Graphene Betavoltaic Isotope Batteries. J. Isot. **37**, 319-326 (2024). doi:10.7538/tws.2024.youxian.035

[13] X.G. Long, G. Huang, S.M. Peng et al., Hydrogen isotope effects of Ti, Zr metals. Fusion Sci. Technol. **60**, 1568-1571 (2023). doi:10.13182/FST11-A12733

[14] W.F. Zhang, S. Liu, L.B. Wang et al., Properties of Ti and Ti-alloy film deposited by direct current magnetron sputtering. At. Energy Sci. Technol. **42**, 933– 937 (2008). doi:10.7538/yzk.2008.42.10.0933

[15] Z.Y.Wang,N. Yao, X. Hu, Structural and Optical Property of Titanium Oxide Film Prepared by Energy Filtering Magnetron Sputtering Technique. Int. J. Appl. Ceram. Technol. **13**, 164-169 (2016). doi:10.1111/ijac.12425

[16] X. Chi, C.H. Song, J.F. Bao et al., Research progress of titanium-based thin films prepared by magnetron sputtering. Therm. Spray Technol. **12**, 17-21 (2020). doi:10.3969/j.issn.1674-7127.2020.02.003

[17] A. Y. Chen, Y. Bu, Y. T. Tang et al., Deposition-rate dependence of orientation growth and crystallization of Ti thin films prepared by magnetron sputtering. Thin Solid Films. **574**, 71–77 (2015). doi:10.1016/j.tsf.2014.10.053

[18] V. Chawla, R. Jayaganthan, A.K. Chawla et al., Microstructural characterizations of magnetron sputtered Ti films on glass substrate. J. Mater. Process. Technol. **209**, 3444-3451 (2009). doi:10.1016/j.jmatprotec.2008.08.004

[19] Y.Z. Han, S.J. Li, X. Li et al., Study on Process Parameters of Magnetron Sputtering Titanium Coating in Deep Porous Structures. ACS Omega. **9**, 14551-14557 (2024). doi:10.1021/acsomega.4c00540

[20] P. Moskovkin, C. Maszl, R. Schierholz et al., Link between plasma properties with morphological, structural and mechanical properties of thin Ti films deposited by high power impulse magnetron sputtering. ACS Omega. **418**, 127235 (2021). doi:10.1016/j.surfcoat.2021.127235

[21] R. Añez, A. Sierraalta, M.A. San-Miguel et al., Role of the Si–Si bond stability in the first stages of Ti diffusion on a Si(1 1 1) 2 × 1 surface A periodic DFT study. Appl. Surf. Sci. **273**, 496-501 (2013). doi:10.1016/j.apsusc.2013.02.068

[22] R. Añez, A. Sierraalta, L. Díaz et al., Periodic DFT study of Ti deposition on defective Si(100) surfaces. Appl. Surf. Sci. **335**, 160-166 (2015). doi:10.1016/j.apsusc.2015.02.046

[23] R. Añez, M.A. San-Miguel and J.F. Sanz, Periodic DFT study of Ti deposition on defective Si(100) surfaces. Surf. Sci. **606**, 754-761 (2012). doi:10.1016/j.susc.2012.01.006

[24] A. Giri, J.L. Braun and P.E. Hopkins, Effect of crystalline/amorphous interfaces on thermal transport across confined thin films and superlattices. J. Appl. Phys. **119**, (2016). doi:10.1063/1.4953683

[25] Y. Gao, Q. Xie, T.H. Gao et al., Investigation of interfacial matching between 3C-SiC substrate crystals and its surface layer deposited Cu elements using molecular dynamics simulations. Surf. Interfaces. **43**, 103600 (2023). doi:10.1016/j.surfin.2023.103600

[26] R. Namakian, B.R. Novak, X.M. Zhang et al., A combined molecular dynamics/Monte Carlo simulation of Cu thin film

growth on TiN substrates: Illustration of growth mechanisms and comparison with experiments. Appl. Surf. Sci. **570**, 151013 (2021). doi:10.1016/j.apsusc.2021.151013

[27] L. Ji, L. Liu, Z.W. Xu et al., Molecular dynamics simulation on the effect of dislocation structures on the retention and distribution of helium ions implanted into silicon. Nanotechnol. Precis. Eng. **3**, 81-87 (2020). doi:10.1016/j.npe.2020.03.003

[28] Y.Y. Liu, Z.H. Shi, T.B. Liang et al., The mechanism of room-temperature oxidation of a HF-etched $Ti_3C_2T_x$ MXene determined via environmental transmission electron microscopy and molecular dynamics. InfoMat. **6**, e12536 (2024). doi:10.1002/inf2.12536

[29] X.L. Li, X. Zhang, Y.H. Xu et al., Molecular dynamics study of surface binding energy and sputtering in W-V alloys. FUSION ENG. DES. **195**, 113971 (2023). doi:10.1016/j.fusengdes.2023.113971

[30] Y. Tang, J.K. Liu, Z.H. Yu et al., Molecular dynamics study on the dependence of thermal conductivity on size and strain in GaN nanofilms. Chin. Phys. B. **32**, 066502 (2023). doi:10.1088/1674-1056/acbf26

[31] T. Li, Molecular dynamics simulations of droplet coalescence and impact dynamics on the modified surfaces: A review. Comput. Mater. Sci. **230**, 112547 (2023). doi:10.1016/j.commatsci.2023.112547

[32] E.C. Neyts, A. Bogaerts, Combining molecular dynamics with Monte Carlo simulations: implementations and applications. Theor. Chem Acc. **132**, 277-288 (2013). doi:10.1007/s00214-012-1320-x

[33] K.M. Bal, E.C. Neyts, On the time scale associated with Monte Carlo simulations. J. Chem. Phys. **141**, (2014). doi:10.1063/1.4902136

[34] A. Papadopoulou, E.D. Becker, M. Lupkowski et al., Molecular dynamics and Monte Carlo simulations in the grand canonical ensemble: Local versus global control. J. Chem. Phys. **98**, 4897-4908 (1993). doi:10.1063/1.464945

[35] J. Zhang, C. Liu, Y.H. Shu et al., Growth and properties of Cu thin film deposited on Si(001) substrate: A molecular dynamics simulation study. Appl. Surf. Sci. **261**, 690-696 (2012). doi:10.1016/j.apsusc.2012.08.082

[36] S.F. Hwang, Y.H. Li and Z.H. Hong, Molecular dynamic simulation for Cu cluster deposition on Si substrate. Comput. Mater. Sci. **56**, 85-94 (2012). doi:10.1016/j.commatsci.2012.01.010

[37] P.E. Blöchl, Projector augmented-wave method. Phys. Rev. B. **50**, 17953 (1994). doi:10.1103/PhysRevB.50.17953

[38] J.M. Hendrik, D.P. James, Special points for Brillouin-zone integrations. Phys. Rev. B. **13**, 5188 (1976). doi:10.1103/PhysRevB.13.5188

[39] S. Plimpton, Fast Parallel Algorithms for Short-Range Molecular Dynamics. J. Comput. Phys. **117**, 1-19 (1995). doi:10.1006/jcph.1995.1039

[40] P. Gabriel, J.T. Garritt, Bond-order potentials for the Ti_3AlC_2 and Ti_3SiC_2 MAX phases. Phys. Rev. B. **100**, 214114 (2019). doi:10.1103/PhysRevB.100.214114

[41] M.I. Mendelev, T.L. Underwood and G.J. Ackland, Development of an interatomic potential for the simulation of defects, plasticity, and phase transformations in titanium. J. Chem. Phys. **145**, 154102 (2016). doi:10.1063/1.4964654

[42] C.R. Hubbard, H.E. Swanson and F.A. Mauer, A Silicon Powder Diffraction Standard Reference Material. J. Appl. Cryst. **8**, 45-48 (1975). doi:10.1107/S0021889875009508

[43] H.D. Wang, M.L. Dong, X. Cui et al., Mechanical properties of nano Ti films with different thickness. J. Mater. Eng. **43**, 50–56 (2015). doi:10.11868/j.issn.1001-4381.2015.11.009

[44] N.I. Plusnin, A.P. Milenin and D.P. Prihod'ko, Formation of the Co/Si(111)7x7 interface:AES- and EELS-study. Appl. Surf. Sci. **166**, 125-159 (2000). doi:10.1016/s0169-4332(00)00393-7

[45] Y.J. Tang, J. Tao, H.J. Tao et al., Effects of deposition parameters on structures of sputtered Ti films and TiO_2 nanotube arrays prepared by anodic oxidation. Rare Metal. Mater. Eng. **37**, 2186–2190 (2008). doi:10.3321/j.issn:1002-185X.2008.12.027

[46] R. Alvarez, A. Garcia-Valenzuela, V. Rico et al., Kinetic energy-induced growth regimes of nanocolumnar Ti thin films deposited by evaporation and magnetron sputtering. Nanotechnology. **30**, 475603 (2019). doi:10.1088/1361-6528/ab3cb2

[47] Y.Y. Cheng, C.C. Lee, Simulation of molecular dynamics associated with surface roughness on an Al thin film. Surf. Coat. Technol. **203**, 918-921 (2008). doi:10.1016/j.surfcoat.2008.08.011

[48] P. Moskovkin, C. Maszl, R. Schierholz et al., Link between plasma properties with morphological, structural and mechanical properties of thin Ti films deposited by high power impulse magnetron sputtering. Surf. Coat. Technol. **418**, 127235 (2021). doi:10.1016/j.surfcoat.2021.127235

[49] R. Shi, V. Dixit, H.L. Fraser et al., Variant selection of grain boundary α by special prior β grain boundaries in titanium alloys. Acta Mater. **75**, 156-166 (2014). doi:10.1016/j.actamat.2014.05.003

[50] N. Stanford, P.S. Bate, Crystallographic variant selection in Ti–6Al–4V. Acta Mater. **52**, 5215-5224. (2004). doi:10.1016/j.actamat.2004.07.034